Journal of Catalysis 266 (2009) 351–358

Contents lists available at ScienceDirect

Journal of Catalysis

journal homepage: www.elsevier.com/locate/jcat

Enhanced metal dispersion and hydrodechlorination properties of a Ni/Al_2O_3 catalyst derived from layered double hydroxides

Jun-Ting Feng, Yan-Jun Lin, David G. Evans, Xue Duan, Dian-Qing Li *

State Key Laboratory of Chemical Resource Engineering, Beijing University of Chemical Technology, Box 98, 15 Bei San Huan East Road, Beijing 100029, China

ARTICLE INFO

Article history:
Received 14 April 2009
Revised 1 July 2009
Accepted 3 July 2009
Available online 30 July 2009

Keywords:
Layered double hydroxides
Highly dispersed
Ni/Al_2O_3
Hydrodechlorination of chlorobenzene

ABSTRACT

An Ni^{2+}—Al^{3+}—CO_3^{2-}-layered double hydroxides (NiAl–LDHs) precursor has been synthesized in the pores of spherical γ-Al_2O_3 particles. After calcination at 500 °C, a NiO/γ-Al_2O_3 catalyst precursor was obtained. X-ray photoelectron spectroscopy, temperature programmed reduction, and temperature programmed desorption of hydrogen showed that in the material prepared by calcination of NiAl–LDHs supported on Al_2O_3, the NiO was characterized by higher reduction temperature, stronger interactions with Al_2O_3, and higher nickel dispersion compared with the NiO in a material prepared by conventional impregnation of γ-Al_2O_3 with an aqueous solution of Ni^{2+} ions followed by calcination at 500 °C. The vapor phase hydrodechlorination of chlorobenzene using molecular hydrogen was studied using Ni/γ-Al_2O_3 catalysts prepared by reduction of the NiO/γ-Al_2O_3 catalyst precursors synthesized by the two different methods. Under identical reaction conditions, the Ni/γ-Al_2O_3 catalyst obtained from the LDHs precursor exhibited not only higher activity but also better stability.

1. Introduction

Chlorinated aromatics and their derivatives play important roles in the fields of chemical engineering, pharmaceuticals, and electronics as materials, intermediates, or organic solvents [1]. These compounds, however, are responsible for many instances of highly toxic industrial waste with the result that increasingly severe and restrictive directives have been issued to regulate their disposal [2,3]. A variety of processes including physical methods, biological methods, chemical oxidation methods, and chemical reduction methods have been reported for their disposal [4,5]. Hydrodechlorination (HDC) is one such method for handling this type of hazardous waste. The HDC process involves a low temperature conversion of the chlorinated component into an easily trapped inorganic form, with no hazardous by-products such as dioxins [6].

Although precious metals have good activity and selectivity in HDC reactions, their price and limited availability restrict their industrial applications. Thus attention has been paid to base metals such as iron, cobalt and, particularly, nickel [7]. Supported nickel catalysts prepared by conventional impregnation methods have an inhomogeneity in Ni^{2+} distribution over the support, owing to the surface tension of the impregnating solution and other solvent effects. Moreover, the weak interactions between the support and metal ion species lead to the migration and aggregation of Ni^{2+} during subsequent calcination at high temperature, resulting in an increase in the inhomogeneity of the Ni^{2+} distribution.

Layered double hydroxides (LDHs) are a class of anionic clays. Their general formula [8,9] can be expressed as $[M^{2+}_{1-x}M^{3+}_x(OH)_2]^{x+}(A^{n-})_{x/n}\cdot mH_2O$, where M^{2+} and M^{3+} are di- and tri- valent metal cations, A^{n-} denotes an organic or inorganic anion with negative charge n, and x (=$[M^{3+}]/([M^{2+}]+[M^{3+}])$) is the value of the stoichiometric coefficient. The M^{2+} and M^{3+} cations are uniformly dispersed within the layers without the formation of 'lakes' of like cations. Thus, these layered materials have been widely used as catalysts, catalyst precursors, or catalyst supports. We have previously shown [10] that NiAl–LDHs films can be prepared by reaction of an alkaline solution of Ni^{2+} ions with porous anodic alumina, which acts as both substrate and sole source of Al^{3+} cations.

In this work, micro-spherical γ-Al_2O_3 with high specific surface area and excellent physical strength was used as a support and sole source of Al^{3+} for the synthesis of Ni^{2+}—Al^{3+}—CO_3^{2-}—LDHs in the pores of the material. Formation of the LDHs resulted from decomposition of urea dissolved in an aqueous solution of Ni^{2+} impregnated into the γ-Al_2O_3. After calcination and reduction, a highly dispersed Ni/γ-Al_2O_3 catalyst was obtained. As a comparison, a Ni/γ-Al_2O_3 catalyst was prepared by a conventional impregnation method, followed by calcination and reduction. The structure and properties of these two catalysts, including their catalytic performance in the gas phase HDC of a typical chlorinated aromatic compound, chlorobenzene (CB), were investigated.

* Corresponding author. Fax: +86 10 64425385.
E-mail address: lidq@mail.buct.edu.cn (D.-Q. Li).

0021-9517/$ - see front matter © 2009 Elsevier Inc. All rights reserved.
doi:10.1016/j.jcat.2009.07.001

2. Experimental

2.1. Materials

$Ni(NO_3)_2{\cdot}6H_2O$, $CO(NH_2)_2$, hydrochloric acid, and hexamethylenetetramine (HMT) were all of A.R. grade, and were used without further purification. The aluminum powder had a purity of 99.6%, and an average particle size of 50 μm. The deionized water used in all experiments had a conductivity of less than 10^{-6} S cm^{-1}.

2.2. Synthesis of spherical alumina

An alumina sol was synthesized by digesting aluminum powder in hydrochloric acid [11]. Aluminum powder (30 g) was dispersed in deionized water (100 mL) in a four-necked flask, followed by slow addition of 15% hydrochloric acid (125 mL) using a peristaltic pump, with vigorous stirring at about reflux temperature. After one-third of the amount of hydrochloric acid had been added into the reactor, a magnetic separation procedure was conducted to remove Fe and Cu impurities through external circulation of the reaction mixture using another peristaltic pump. The final alumina sol contained 12.7% aluminum with an Al/Cl molar ratio of 1.8.

A solution of 40% HMT (14.6 g) was added dropwise to the alumina sol (50.0 g) below 10 °C. Micro-spherical gel particles were prepared by dispersing the resulting mixed sol in a column filled with 500SN heavy distillate oil at 85–95 °C by means of a drop distributor [12]. The resulting gel particles were immersed in the oil, and were aged at 140–145 °C for 4–6 h at 0.5–0.6 MPa in order to decompose the HMT completely. Any NH_4Cl remaining in the pores of the hydrated alumina microspheres was thoroughly removed by washing using deionized water. The samples were dried at 120 °C until there was no further weight loss. After calcination at 600 °C for 4 h in air, spherical γ-Al_2O_3 particles were obtained.

2.3. Preparation of NiAl–LDHs/γ-Al_2O_3

$Ni(NO_3)_2{\cdot}6H_2O$ (4.37 g) and urea (1.80 g) were dissolved in 5 mL of deionized water to obtain about 10 mL of mixed solution. The resulting solution was then added to a four-necked flask with 5 g of spherical γ-Al_2O_3 particles. After being impregnated for 1 h about 3 mL of solution remained, with the balance having being absorbed by the spherical γ-Al_2O_3 particles. The particles together with the residual solution were transferred to an autoclave and aged at 120 °C for 24 h, and were then thoroughly washed with deionized water until the pH value of the washings reached 7. The resulting NiAl–LDHs/γ-Al_2O_3 catalyst precursor was obtained after drying at 70 °C for 12 h.

2.4. Preparation of $Ni(NO_3)_2$/γ-Al_2O_3

Five grams of γ-Al_2O_3 were added to 5 mL of 3 mol L^{-1} $Ni(NO_3)_2$ solution and then impregnated for 12 h. The resulting $Ni(NO_3)_2$/γ-Al_2O_3 catalyst precursor was obtained after drying at 70 °C for 12 h.

2.5. Synthesis of pristine NiAl–LDHs

Pristine NiAl–LDHs were prepared as reference samples by means of a method using separate nucleation and aging steps (SNAS) [13]. $Ni(NO_3)_2{\cdot}6H_2O$ and $Al(NO_3)_3{\cdot}9H_2O$ with a Ni^{2+}/Al^{3+} molar ratio of 2:1 were dissolved in deionized water to make a mixed salt solution ($[Ni^{2+}] + [Al^{3+}] = 0.66$ mol L^{-1}). NaOH and Na_2CO_3 were dissolved in deionized water to make an alkali solution ([NaOH] = 1.5 mol L^{-1}, $[Na_2CO_3] = 0.7$ mol L^{-1}). The two solutions were added simultaneously to a modified colloid mill operating with a rotation speed of about 4000 r min^{-1} under N_2 protection [14]. The resulting slurry was transferred to a four-necked flask as quickly as possible and was aged at 40 °C for 15 h with vigorous stirring in a flowing N_2stream. The precipitate was centrifuged and thoroughly washed with deionized water until the pH value of the filtrate reached 7. The final NiAl–LDHs were obtained after drying at 70 °C for 12 h.

2.6. Synthesis of NiO/γ-Al_2O_3 catalyst precursors

The precursors NiAl–LDHs/γ-Al_2O_3 and $Ni(NO_3)_2$/γ-Al_2O_3 were heated in air with a ramping rate of 10 °C min^{-1} to 500 °C and calcined at that temperature for 4 h, followed by slow cooling to room temperature. The two different samples of NiO/γ-Al_2O_3 are denoted U-NiO/γ-Al_2O_3 and I-NiO/γ-Al_2O_3, respectively.

2.7. Analysis and characterization

Powder XRD patterns were recorded on a Shimadzu XRD-600 X-ray powder diffractometer (Cu K_a radiation, $\lambda = 0.15406$ nm) between 3° and 70°, with a scan speed of 10 °C min^{-1}. Elemental analysis was performed using a Shimadzu ICPS-75000 inductively coupled plasma emission spectrometer (ICP-ES) and an Elementar Vario EL elemental analyzer. The morphology, structure, and grain size of the samples were examined using a Hitachi S-4700 scanning electron microscope (SEM). The low temperature N_2 adsorption–desorption experiments were carried out using a Quantachrome Autosorb-1 system. The BJH method was used to calculate pore volume and the pore size distribution. Surface elemental analysis was performed using an ESCALAB250 X-ray photoelectron spectroscopy (XPS). ^{27}Al MAS-NMR analysis was performed using a Bruker AV300 NMR equipment.

Temperature programmed reduction (TPR) and hydrogen temperature programmed desorption (H_2-TPD) of the catalysts were conducted on a Micromeritics ChemiSorb 2720. About 200 mg of NiO/γ-Al_2O_3 samples was loaded in a quartz reactor and heated at 300 °C for 2 h in argon. TPR was carried out with a heating ramp rate of 5 °C min^{-1} in a stream of 10% H_2 in Ar, with a total flow rate of 40 mL min^{-1}. The outlet gas was passed through a cold trap to remove the moisture produced during reduction. TPD was carried out in a stream of argon with a flow rate of 40 mL min^{-1} and a temperature ramp of 10 °C min^{-1}. Hydrogen consumption due to the reduction of NiO was monitored by a thermal conductivity detector (TCD) linked to a computer data acquisition system. The TCD signals were calibrated using Ag_2O as a standard. The Ni metal surface area, dispersion, and crystallite size were calculated from the volume of H_2 chemisorbed using the following simplified equations [15]:

Ni metal surface area:

$$\mathrm{SA_{Ni}(m^2/g\text{-}Cat.)} = \frac{Vad}{Ws \times Vm} \times SF \times N \times RA \tag{1}$$

Ni metal specific surface area:

$$\mathrm{SA_{Ni}(m^2/g\text{-}Ni.)} = \frac{\mathrm{SA(m^2/g)}}{F_{Ni}} \tag{2}$$

Ni dispersion (D):

$$D = \frac{Vad}{Ws} \times \frac{FW_{Ni} \times SF}{F_{Ni} \times Vm} \times 100 \tag{3}$$

Ni metal crystallite size (MCS)

$$\mathrm{MCS} = \frac{6 \times 10^3}{\mathrm{SA_{Ni}(m^2/g\text{-}Ni)} \times d_{Ni}} \tag{4}$$

where Vad = volume of H_2 chemisorbed at STP (mL) to form a monolayer, Ws = weight of the sample (g), Vm = molar volume of H_2 gas

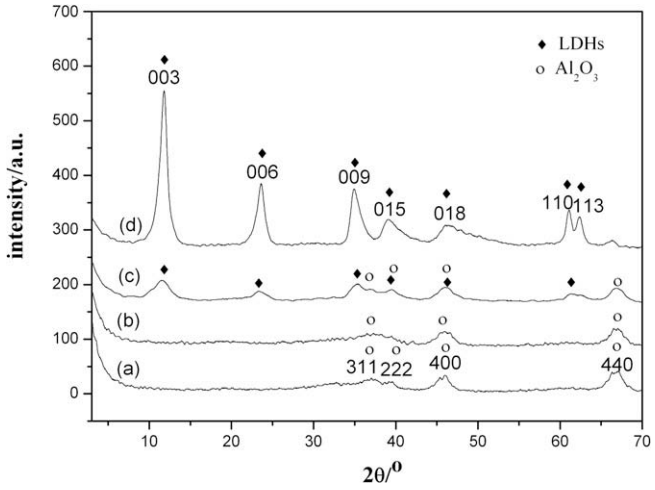

Fig. 1. XRD patterns of γ-Al_2O_3 (a), $Ni(NO_3)_2/\gamma$-Al_2O_3 (b), NiAl–LDHs/γ-Al_2O_3 (c), and NiAl–LDHs (d).

Table 1
Analysis of XRD patterns for NiAl–LDHs/γ-Al_2O_3 and NiAl–LDHs.

Property	NiAl–LDHs/γ-Al_2O_3	NiAl–LDHs
d_{003} (nm)	0.76	0.75
d_{006} (nm)	0.38	0.38
d_{009} (nm)	0.24	0.25
d_{110} (nm)	0.15	0.15
$W_{1/2}$ for [003] (°)	1.47	0.70
$W_{1/2}$ for [110] (°)	0.52	0.36
Lattice parameter a (nm)	0.30	0.30
Lattice parameter c (nm)	2.28	2.25
Crystallite size in direction a (nm)	17.56	25.63
Crystallite size in direction c (nm)	5.37	11.27

(22414 mL mol^{-1}), SF = stoichiometric factor (the Ni:H ratio in the chemisorption) which is taken as 1, $N = 6.023 \times 10^{23}$ Ni atoms mol^{-1}, RA = atomic cross-sectional area of Ni (0.0649 nm^2), F_{Ni} = weight fraction of Ni in the sample as determined by ICP-AES, FW_{Ni} = formula weight of Ni (58.71 g mol^{-1}), and d_{Ni} = density of Ni metal (8.9 g cm^{-3}).

2.8. Catalytic activity tests

All the catalytic reactions were carried out in an Xq WFS-3015 fixed bed microreactor over the temperature range 250–400 °C. About 0.5 g of NiO/γ-Al_2O_3 catalyst precursor was placed in a quartz tubular reactor (7 mm i.d.) between two quartz plugs. Before starting the reaction, the catalyst was pretreated at 400 °C for 2 h in hydrogen with a flow rate of 40 mL min^{-1} and cooled to the required reaction temperature. CB (1.2 mL h^{-1}) was fed into the reactor using an Elite P230 microfeeder and the hydrogen flow was maintained by a mass flow controller. A space velocity (GHSV) of 3360 h^{-1} was maintained throughout the reaction. The reactants and products were analyzed by GC with a flame ionization detector online. Catalytic activity is discussed in this paper in terms of the fractional conversion (x) [16],

$$x = \frac{(mC_6H_5Cl)i - (mC_6H_5Cl)o}{(mC_6H_5Cl)i} \quad (5)$$

where m denotes the number of moles of reactant entering (subscript i) and exiting (subscript o) the reactor per unit time.

3. Results and discussion

3.1. Structure and porosity of NiAl–LDHs/γ-Al_2O_3 and $Ni(NO_3)_2$/γ-Al_2O_3

The powder XRD patterns for γ-Al_2O_3, $Ni(NO_3)_2/\gamma$-Al_2O_3, NiAl–LDHs/γ-Al_2O_3, and NiAl–LDHs are shown in Fig. 1a–d, respectively. The characteristic (311), (222), (400), and (440) reflections of γ-Al_2O_3 can be observed in Fig. 1a [17], and the pattern for $Ni(NO_3)_2/\gamma$-Al_2O_3 shown in Fig. 1b is very similar. The XRD pattern in Fig. 1d is similar to those reported in the literature for LDH phases [9]; the peaks at low angle arise from the basal (003) and higher order (006 and 009) reflections, and the peak around 60° 2θ arises from the (110) reflection. The pattern of NiAl–LDHs/γ-Al_2O_3 is a superposition of the characteristic reflections of γ-Al_2O_3 and those of LDHs as shown in Fig. 1c, which confirms that NiAl–LDHs has been formed on the γ-Al_2O_3 support. The corresponding structural parameters are listed out in Table 1. The lattice parameters a (=2 d_{110}) and c (=$d_{003} + 2d_{006} + 3d_{009}$) of NiAl–LDHs/$\gamma$-$Al_2O_3$ were close to those of the pristine LDHs. According to the Scherrer formula, the crystallite sizes in the a and c-directions can be calculated from

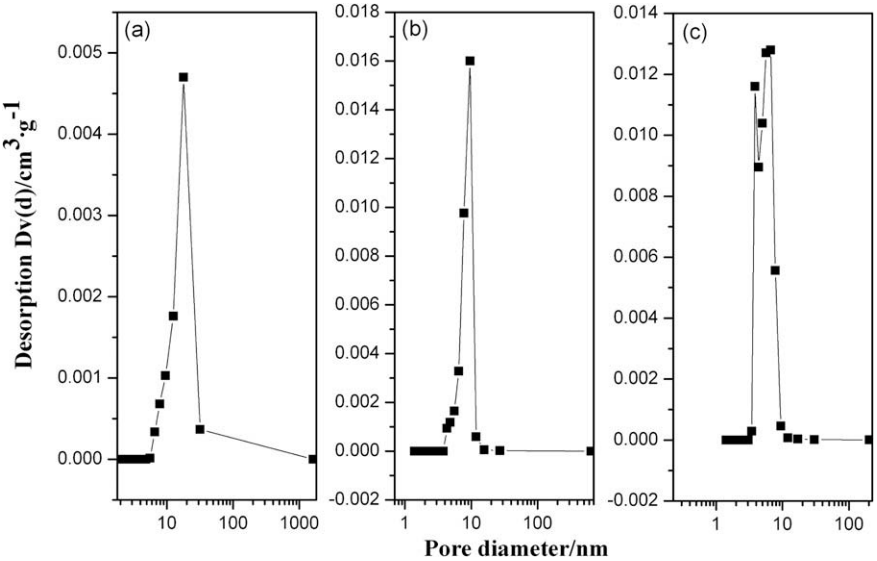

Fig. 2. Curves of pore size distribution of γ-Al_2O_3 (a), $Ni(NO_3)_2/\gamma$-Al_2O_3 (b), and NiAl–LDHs/γ-Al_2O_3 (c).

Table 2
Textural properties of the samples.

Sample	Specific surface area ($m^2\ g^{-1}$)	Most probable pore size (nm)	Total pore volume ($cm^3\ g^{-1}$)
γ-Al_2O_3	179	18.1	0.89
$Ni(NO_3)_2/\gamma$-Al_2O_3	95	9.5	0.50
NiAl–LDHs/γ-Al_2O_3	218	6.2	0.43

the full width at half-height ($W_{1/2}$) of the (110) and (003) reflections, respectively. It is interesting to observe that the crystallite size of NiAl–LDHs grown on γ-Al_2O_3 was much smaller than that of the pristine LDHs. This can be attributed to the confinement effects of the pores of γ-Al_2O_3.

The N_2 adsorption–desorption isotherms of the obtained Al_2O_3, $Ni(NO_3)_2/\gamma$-Al_2O_3, and NiAl–LDHs/γ-Al_2O_3 were all of Type IV with an obvious hysteresis loop [18]. The shape of the hysteresis loop in each case was a superposition of Types H1 and H3. This is generally taken to indicate that samples have both tubular and parallel slit-shaped capillary pores which are caused by the gas escaping during calcination and the stacking of alumina microcrystallites [19]. The corresponding pore size distributions are shown in Fig. 2, and the textural properties are listed out in Table 2. The specific surface area, most probable pore size, and total pore volume of $Ni(NO_3)_2/\gamma$-Al_2O_3 were all significantly smaller than the corresponding values for γ-Al_2O_3. This may be because a large number of $Ni(NO_3)_2$ microcrystallites aggregated together during the drying process and the aggregations blocked some of the pores in the γ-Al_2O_3 support. In the case of NiAl–LDHs/γ-Al_2O_3, the specific surface area was higher than that of γ-Al_2O_3 itself; this may be attributed to the formation of NiAl–LDHs microcrystallites, with regular size and well-developed two-dimensional pores, on the surfaces of γ-Al_2O_3 pores. The total pore volume and the most probable pore size were lower than the corresponding values for γ-Al_2O_3, the reason being that a fraction of the γ-Al_2O_3 pore volume was taken up by NiAl–LDHs microcrystallites.

3.2. Morphology of NiAl–LDHs/γ-Al_2O_3 and $Ni(NO_3)_2/\gamma$-Al_2O_3

A cross-section SEM image of $Ni(NO_3)_2/\gamma$-Al_2O_3 (see Fig. 3a) shows that congeries of $Ni(NO_3)_2$ particles with a size of 10–50 nm blocked most of the pores on the surface of γ-Al_2O_3, and that the nickel-containing phase exhibited low dispersion. In NiAl–LDHs/γ-Al_2O_3 (Fig. 3b), NiAl–LDHs microcrystallites having good crystallinity and uniform size grew homogeneously in the pores and on the surface of γ-Al_2O_3. The crystallite size of NiAl–LDHs in the *c*-direction was 5–15 nm, which is consistent with the XRD results.

The ^{27}Al MAS-NMR analysis indicated that both NiAl–LDHs/γ-Al_2O_3 and γ-Al_2O_3 displayed two resonances at ~6 and ~60 ppm; these chemical shifts are characteristic of AlO_6 octahedra and AlO_4 tetrahedra, respectively, [20]. The ^{27}Al peak intensities for NiAl–LDHs/γ-Al_2O_3 were much lower than those for γ-Al_2O_3, which might be due to the presence of the paramagnetic Ni^{2+} ions. The ratio of AlO_6 to AlO_4 peak areas for NiAl–LDHs/γ-Al_2O_3 was larger than that for γ-Al_2O_3. This indicates that rather than being simply supported on the γ-Al_2O_3, NiAl–LDHs microcrystallites were chemically grafted via bonding of (Ni-coordinated) O atoms with AlO_4 tetrahedra, resulting in the formation of additional AlO_6 octahedra via Al–O–Ni linkages.

3.3. Structure and porosity of NiO/γ-Al_2O_3 catalyst precursors

Powder XRD patterns for γ-Al_2O_3, I-NiO/γ-Al_2O_3, and U-NiO/γ-Al_2O_3 are shown in Fig. 4a–c, respectively. The characteristic (311), (222), (400), and (440) reflections of γ-Al_2O_3; the characteristic (111) and (220) reflections of NiO (bunsenite); and the characteristic (311) reflection of $NiAl_2O_4$ spinel [21] can be observed in Fig. 4b and c. This demonstrates that both $Ni(NO_3)_2$ and NiAl–LDHs supported on γ-Al_2O_3 were transformed into NiO and $NiAl_2O_4$ after calcination at 500 °C.

The isotherms of both samples of NiO/γ-Al_2O_3 were all of Type IV, like those of the uncalcined precursors, with an obvious hyster-

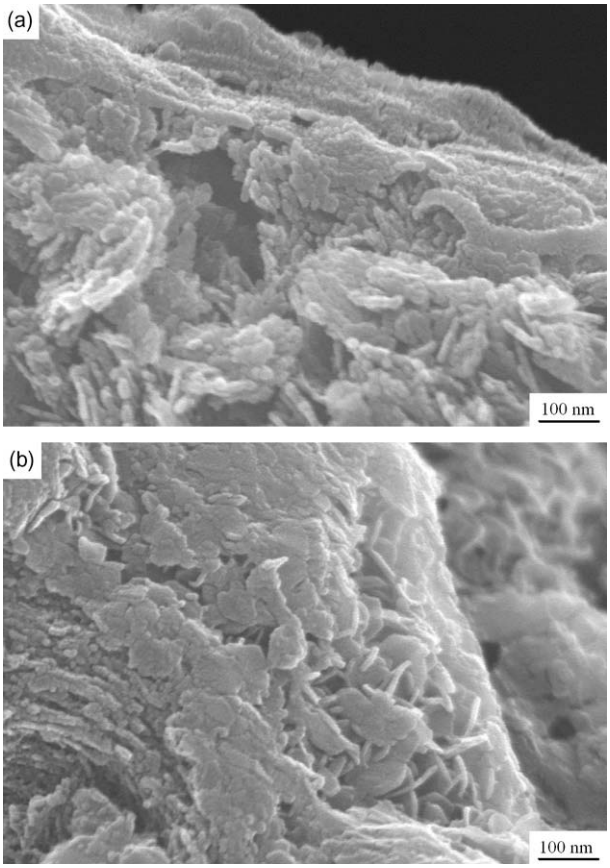

Fig. 3. SEM micrographs of cross-sections of $Ni(NO_3)_2/\gamma$-Al_2O_3 (a) and NiAl–LDHs/γ-Al_2O_3 (b).

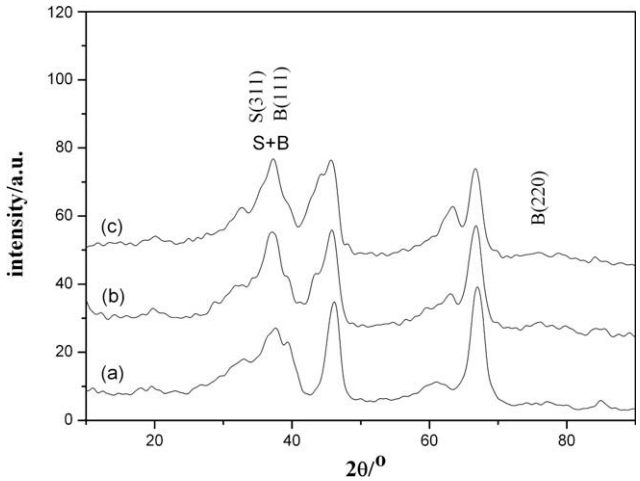

Fig. 4. XRD patterns of γ-Al_2O_3 (a), I-NiO/γ-Al_2O_3 (b), and U-NiO/γ-Al_2O_3 (c) B-NiO (bunsenite), S-$NiAl_2O_4$ (spinel).

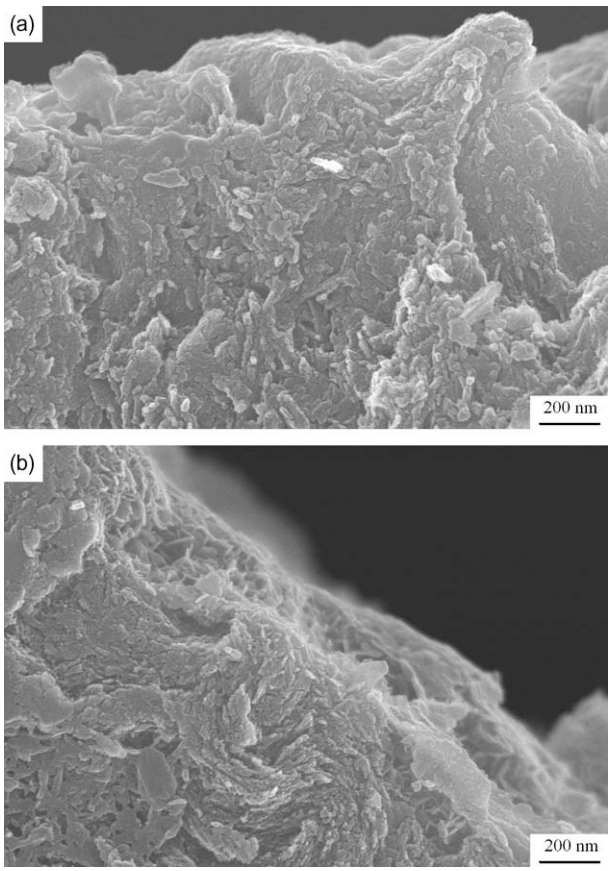

Fig. 5. SEM micrographs of cross-sections of I-NiO/γ-Al_2O_3 (a) and U-NiO/γ-Al_2O_3 (b).

esis loop which was a superposition of Types H1 and H3. The total pore volume and the most probable pore size of U-NiO/γ-Al_2O_3 (0.52 $cm^3\ g^{-1}$ and 11.9 nm) were slightly higher than the corresponding values for the NiAl–LDHs/γ-Al_2O_3 precursor (Table 2), whilst the specific surface area (193 $m^2\ g^{-1}$) was somewhat lower. This may be because the decomposition of layer hydroxyl groups and interlayer carbonate anions in NiAl–LDHs, with associated loss of water and carbon dioxide, led to a decrease in the size of the particles after calcination, and the resulting Ni/Al mixed oxides therefore took up less of the pore volume of γ-Al_2O_3 than the NiAl–LDHs precursor. In the case of I-NiO/Al_2O_3, the specific surface area (138 $m^2\ g^{-1}$), most probable pore size (7.8 nm), and total pore volume (0.65 $cm^3\ g^{-1}$) were all significantly higher than the corresponding values for Ni$(NO_3)_2$/γ-Al_2O_3 (Table 2). The increase in surface area may result from decomposition of Ni$(NO_3)_2$, with relatively low surface area, to afford NiO with much smaller particle size. The increased pore size and total pore volume suggest that some new pores were generated in the calcination process; these may be caused by the weak interactions between the γ-Al_2O_3 support and the Ni species leading to accumulation of NiO particles.

3.4. Morphology of NiO/γ-Al_2O_3 catalyst precursors

Cross section SEM micrographs of I-NiO/γ-Al_2O_3 and U-NiO/γ-Al_2O_3 are shown in Fig. 5. In the case of I-NiO/γ-Al_2O_3, a large quantity of NiO was congregated on the surface of γ-Al_2O_3, as shown in Fig. 5a, which can be attributed to the migration of Ni^{2+} during drying and calcination processes. In contrast, in the case of U-NiO/γ-Al_2O_3, NiO particles were dispersed homogeneously on the surface and pores of γ-Al_2O_3 as shown in Fig. 5b. These micrographs clearly confirm that U-NiO/γ-Al_2O_3 possessed higher surface dispersion than I-NiO/γ-Al_2O_3.

3.5. XPS study of NiO/γ-Al_2O_3 catalyst precursors

Several XPS studies of oxidized and reduced forms of supported and unsupported nickel catalysts have been reported in the literature [22,23]. As shown in Fig. 6, the XPS spectra of I-NiO/γ-Al_2O_3 and U-NiO/γ-Al_2O_3 in the Ni $2p_{3/2}$ region were essentially identical. Both contained three peaks, appearing at binding energies around 855, 856, and 862 eV, suggesting that there were three different Ni sites on the γ-Al_2O_3 support. The first peak located at around 855 eV can be attributed to the binding energy of Ni $2p_{3/2}$ in NiO dispersed on γ-Al_2O_3 [24]. The second peak centered at 856 eV is characteristic of Ni $2p_{3/2}$in NiO particles interacting more strongly with the carrier [24]. Comparison of the ratios of the area of the second peak to that of first peak between the two spectra

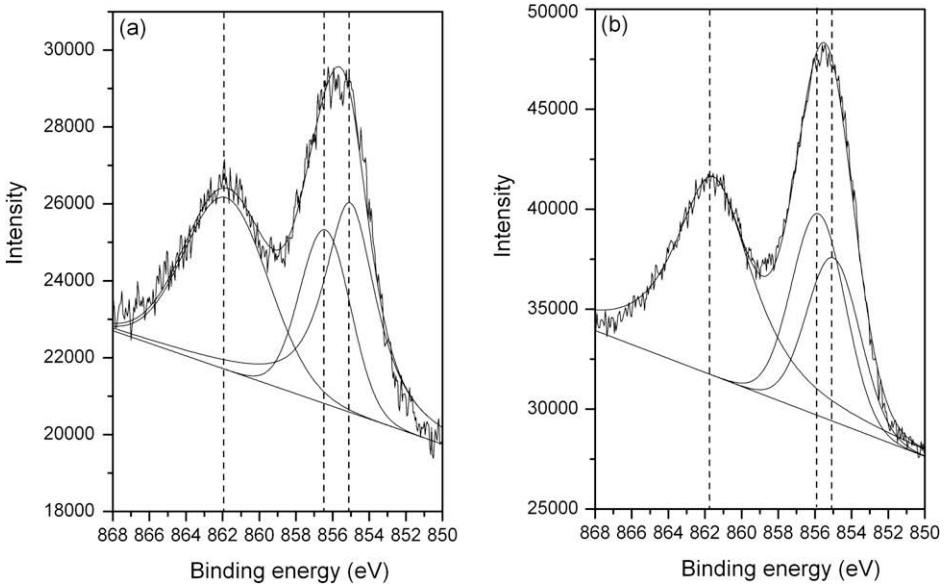

Fig. 6. XPS spectra of the Ni $2p_{3/2}$ region of I-NiO/γ-Al_2O_3 (a) and U-NiO/γ-Al_2O_3 (b).

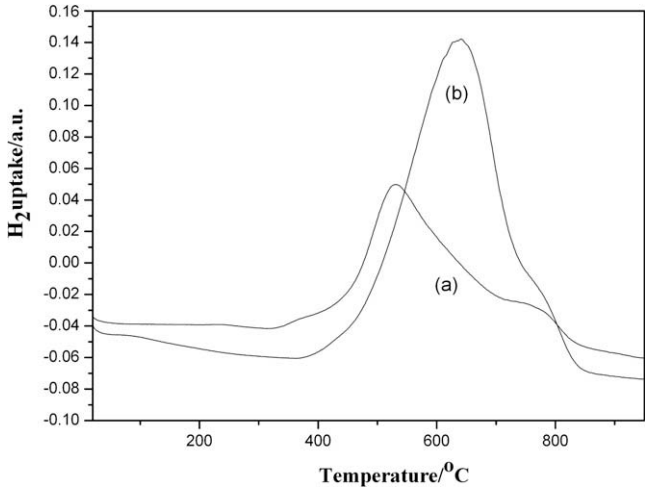

Fig. 7. TPR profiles of I-NiO/γ-Al_2O_3 (a) and U-NiO/γ-Al_2O_3 (b).

illustrates that the interaction between NiO and γ-Al_2O_3 in U-NiO/γ-Al_2O_3 is much stronger than that in I-NiO/γ-Al_2O_3. The peak located at round 862 eV can be assigned to Ni^{2+} ions in a network of $Ni(OH)_2$, $NiAl_2O_3$, and $NiAl_2O_4$ compounds [25].

3.6. TPR and H_2-TPD studies of NiO/γ-Al_2O_3 catalyst precursors

TPR profiles obtained for the NiO/γ-Al_2O_3 catalyst precursors are shown in Fig. 7. The TPR traces for both I-NiO/γ-Al_2O_3 and U-NiO/γ-Al_2O_3 showed two peaks. The peak below 700 °C can be attributed to the reduction of NiO particles and, in both cases, occurred at a much higher temperature than the corresponding peak for pure NiO, which occurs around 370 °C [26]. This implies the presence of strong interactions between NiO and γ-Al_2O_3. The higher temperature peak is consistent with the reduction of a $NiAl_2O_4$ spinel or strongly interacting NiO-γ-Al_2O_3 phase; the presence of such phases was indicated by XPS. The reduction temperature and peak area for I-NiO/γ-Al_2O_3 were lower than the corresponding values for U-NiO/γ-Al_2O_3, which could be due to the larger crystallite size in the former leading to incomplete reduction of NiO particles [27].

H_2-TPD experiments were performed in order to obtain information about the surface structure of the catalysts as well as to determine quantitatively the amount of chemisorbed hydrogen; the latter is a good indication of the degree of metal dispersion and surface area. H_2-TPD profiles from 120 °C to 950 °C of I-NiO/γ-Al_2O_3 and U-NiO/γ-Al_2O_3 are shown in Fig. 8 (any peaks below 120 °C can be attributed to physical desorption). Both the profiles showed at least two domains of H_2 desorption peaks. Peaks below 700 °C are generally attributed to H_2 desorbed from metal particles and therefore indicate the exposed fraction of Ni atoms, whilst high temperature peaks are attributed to H_2 located in subsurface layers and/or to spillover H_2 [28,29]. Hydrogen uptake values and other related properties calculated from the desorption measurements on the Ni/Al_2O_3 catalysts are given in Table 3, along with the nickel loading as determined by ICP. The value of the Ni loading in U-Ni/γ-Al_2O_3 was very similar to that in the synthesis mixture (15 wt.%), whereas the Ni loading in I-Ni/γ-Al_2O_3 was lower than the value in the synthesis mixture (also 15 wt.%), which indicates loss of Ni during the preparation of the latter material. The Ni dispersion in U-Ni/γ-Al_2O_3 was significantly higher than that in I-Ni/γ-Al_2O_3.

3.7. Catalytic HDC of CB

HDC of CB was carried out using U-Ni/γ-Al_2O_3 and I-Ni/γ-Al_2O_3, prepared by hydrogen reduction of the corresponding NiO/γ-Al_2O_3 precursors, as catalysts under a variety of conditions.

3.7.1. Influence of reaction temperature on the activity of HDC of CB

The catalytic performances of U-Ni/γ-Al_2O_3 and I-Ni/γ-Al_2O_3 during the vapor phase HDC of CB at different temperatures for 3 h, with H_2, N_2, and CB flow velocities of 13.4, 40.2, and 0.03 mL min^{-1}, respectively, are shown in Fig. 9. HDC of CB normally results in the production of three products, *viz.* benzene, cyclohexane, and chlorocyclohexane [30]. U-Ni/γ-Al_2O_3 exhibited

Table 3
Analytical data and hydrogen adsorption properties of Ni/Al_2O_3 catalysts.

Sample	Ni loading[a] (%)	H_2 uptake (mL g^{-1} STP)	Dispersion (%)	Crystallite size (nm)	Ni specific surface area (m^2 g^{-1})
I-Ni/γ-Al_2O_3	13.2	2.5	22.2	4.6	148
U-Ni/γ-Al_2O_3	15.0	3.3	28.6	3.6	190

[a] As determined by ICP.

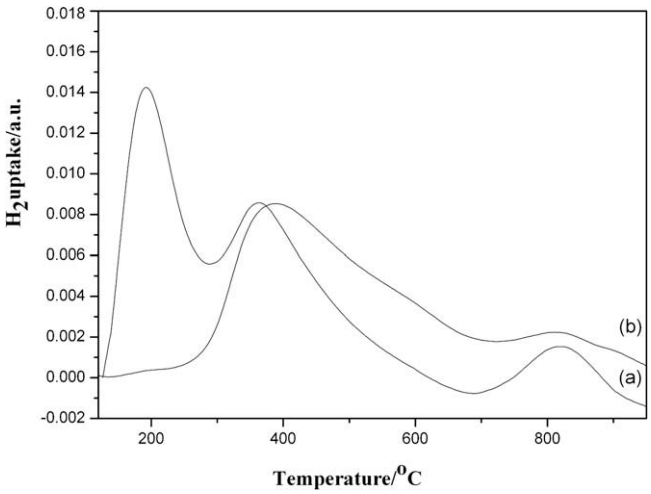

Fig. 8. H_2-TPD profiles of I-NiO/γ-Al_2O_3 (a) and U-NiO/γ-Al_2O_3 (b).

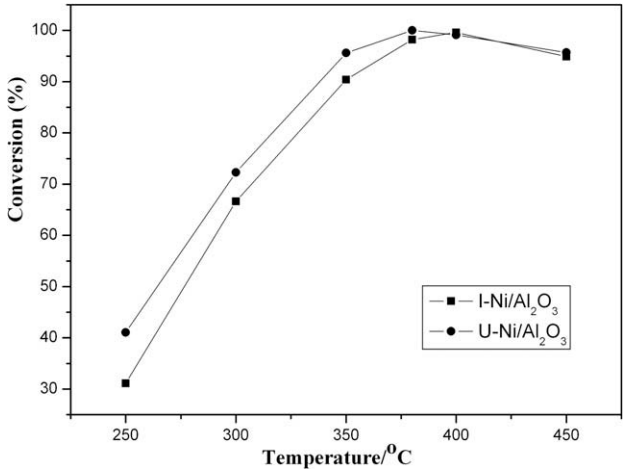

Fig. 9. Effect of varying the reaction temperature on HDC of CB over the Ni/Al_2O_3 catalysts prepared with nominal 15 wt.% Ni.

higher catalytic activity than I-Ni/γ-Al_2O_3 over the temperature range 250–380 °C, which can be attributed to the smaller crystallite size, higher Ni dispersion, and higher surface area of the former (the masses of the two catalysts used were scaled according to their composition to ensure that identical amounts of nickel were present in each case). HDC of CB in the presence of the U-Ni/γ-Al_2O_3 catalyst over the temperature range 250–380 °C produced benzene as the only significant product, and the conversion of CB reached 100% at 380 °C. When the reaction temperature was raised above 380 °C, cyclohexane was detected and there was a decrease in the conversion of CB. The same trends were observed for I-Ni/γ-Al_2O_3.

3.7.2. Influence of the hydrogen partial pressure on catalytic activity

Fig. 10 depicts the effect of varying the hydrogen partial pressure in HDC of CB. N_2/H_2 molar ratios of 4:1, 3:1, 2:1, and 1:1 were employed in the experiments, which were carried out at 370 °C for 3 h with a total flow velocity of 53.6 mL min^{-1}. It was observed that for both U-Ni/γ-Al_2O_3 and I-Ni/γ-Al_2O_3, the conversion of CB increased when the N_2/H_2 molar ratio was decreased from 4:1 to 2:1. However, over-hydrogenation of CB to cyclohexane was found at higher H_2 pressures. Thus, a N_2/H_2 molar ratio of 2:1 is optimal for HDC of CB.

3.7.3. Effect of Ni content on the activity of HDC of CB

The activities for HDC of CB at 370 °C for 3 h, with H_2, N_2, and CB flow velocities of 13.4, 40.2, and 0.03 mL min^{-1}, respectively, over U-Ni/γ-Al_2O_3 and I-Ni/γ-Al_2O_3 prepared using different loadings of nickel are reported in Fig. 11. For both catalysts, the activity increased with increasing Ni content. This is consistent with the results reported by Suzdorf et al. in their study of Ni/Al_2O_3 as a catalyst for HDC of CB [31]. Catalysts with nominal 15 wt.% nickel loading were used in the subsequent stability study.

3.7.4. Time-on-stream analysis

Catalyst deactivation is generally a problem in the HDC reaction,and it has been attributed mainly to the presence of HCl generated in the reaction, which leads to the formation of a stable surface chloride species; the reaction then becomes a cycle of chlorination/dechlorination of the surface [27]. Fig. 12 shows the results of time-on-stream analyses for U-Ni/γ-Al_2O_3 and I-Ni/γ-Al_2O_3 catalysts containing about 15 wt.% Ni at 370 °C with H_2, N_2, and CB flow velocities of 13.4, 40.2, and 0.03 mL min^{-1}, respectively. The two Ni/γ-Al_2O_3 catalysts had very high initial activity,

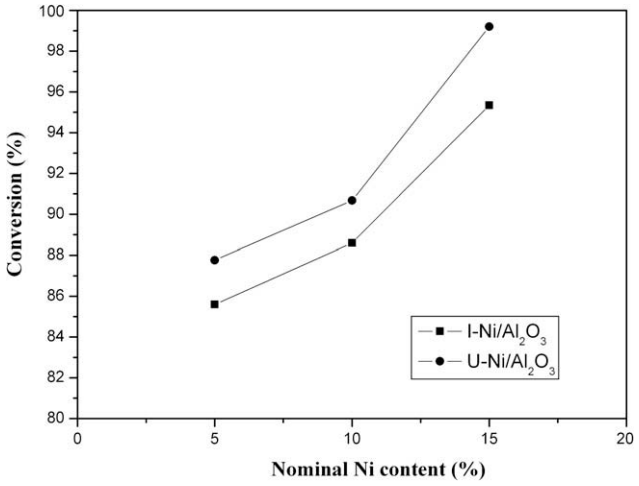

Fig. 11. Effect of varying the nominal Ni content in the Ni/Al_2O_3 catalysts on HDC of CB.

approaching 99.8% conversion of CB. The U-Ni/γ-Al_2O_3 catalyst exhibited better stability, maintaining about 99.0% conversion after attaining a steady state within a period of 4 h on stream, whereas the I-Ni/γ-Al_2O_3 catalyst reached a steady state conversion of only ca. 95% after 6 h on stream. The enhanced stability of U-Ni/γ-Al_2O_3 is consistent with its smaller crystallite size, higher Ni dispersion, and the stronger interaction between the Ni species and the γ-Al_2O_3 support.

The spent catalysts were also characterized by ICP, XRD, TPR, and H_2-TPD. ICP results indicated no evidence for Ni loss of either catalyst during the reaction. The characteristic reflections of $NiCl_2$ can be observed in the XRD pattern of the used catalyst I-Ni/γ-Al_2O_3, which indicated the poisoning of active nickel species with HCl produced during HDC reaction. This can be ascribed to the weak interactions between Ni species and γ-Al_2O_3 support in the I-Ni/γ-Al_2O_3 catalyst. In contrast, the used catalyst U-Ni/γ-Al_2O_3 did not show any new peaks in its XRD pattern. The spent U-Ni/γ-Al_2O_3 catalyst exhibited similar TPR and H_2-TPD traces to the fresh catalyst, with slightly lower peak areas than the fresh catalyst. This illustrates that the metal dispersion of the U-Ni/γ-Al_2O_3 catalyst decreased only marginally during the HDC reaction

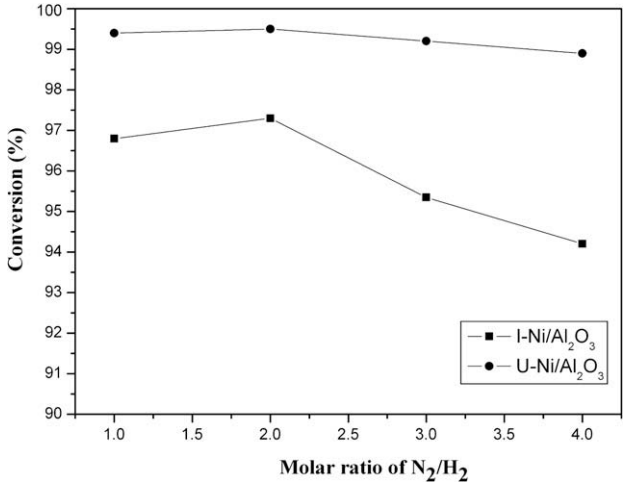

Fig. 10. Conversion of CB at different H_2 partial pressures over the Ni/Al_2O_3 catalysts prepared with nominal 15 wt.% Ni.

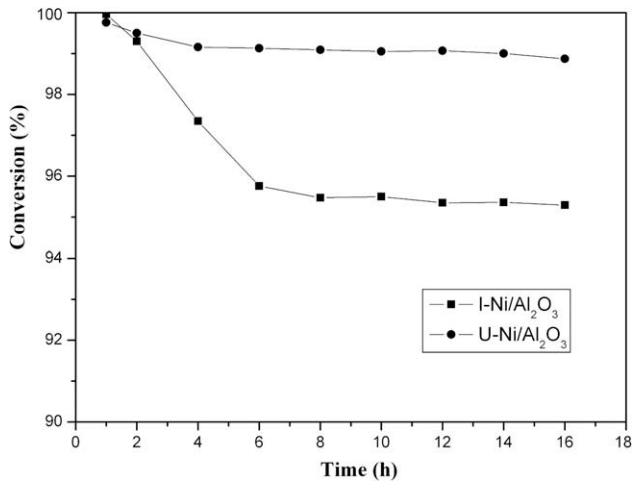

Fig. 12. Time-on-stream analysis: HDC of CB over nominal 15 wt.% Ni/Al_2O_3 catalysts.

because of a small quantity of metal atom sintering. Therefore, the deactivation of the U-Ni/γ-Al_2O_3 catalyst was relatively low. In the case of the I-Ni/γ-Al_2O_3 catalyst, the used catalyst exhibited two extra reduction peaks due to the formation of the $NiCl_2$ phase, and had a significantly lower peak area in the H_2-TPD trace than the fresh catalyst, which indicates that the extent of metal dispersion decreased markedly during the HDC reaction. Thus, the deactivation observed for the I-Ni/γ-Al_2O_3 catalyst can be attributed not only to the poisoning of active nickel species with HCl, but also to the sintering of metal atoms [27,32].

4. Conclusions

Spherical γ-Al_2O_3 particles with high specific surface area and well-developed pore canals were prepared by the oil column method and were used as support and sole Al source for the synthesis of Ni^{2+}—Al^{3+}—CO_3^{2-}—LDHs microcrystallites within the pore canals of the material. XRD, SEM, and BET measurements indicated that the crystallite size of NiAl–LDHs grown within the pores of γ-Al_2O_3 was smaller than that of pristine NiAl–LDHs prepared by conventional co-precipitation. The specific surface area of NiAl–LDHs/γ-Al_2O_3 was higher than that of the γ-Al_2O_3 precursor due to the well-developed two-dimensional pores of NiAl–LDHs. After calcination at 500 °C, an alumina-supported nickel oxide species (denoted U-NiO/Al_2O_3) was obtained. As a comparison, an alumina-supported nickel oxide species (denoted I-NiO/Al_2O_3) was prepared by a conventional impregnation method, followed by calcination at 500 °C. SEM, BET, and XPS analyses showed that U-NiO/Al_2O_3 possessed higher nickel dispersion and specific surface area than I-NiO/Al_2O_3, as well as stronger interactions between NiO and Al_2O_3. TPR and H_2-TPD analyses indicated that the Ni dispersion and Ni specific surface area of U-Ni/Al_2O_3were significantly higher than those of I-Ni/Al_2O_3.

Studies of the vapor phase HDC of CB with U-Ni/Al_2O_3 and I-Ni/Al_2O_3, prepared by hydrogen reduction of the corresponding NiO precursors, showed that high reaction temperatures (>380 °C) or high H_2 partial pressures led to over-hydrogenation of CB to afford cyclohexane. The activity of both catalysts increased with increasing Ni content. U-Ni/γ-Al_2O_3 exhibited higher activity, selectivity, and stability than I-Ni/γ-Al_2O_3 due to its smaller crystallite size, higher Ni dispersion, and stronger interaction between Ni species and the γ-Al_2O_3 support. U-Ni/γ-Al_2O_3 catalysts with about 15 wt.% Ni showed optimal activity and selectivity at 380 °C with a N_2/H_2 molar ratio of 2:1.

Acknowledgment

This work was supported by National Key Natural Science Research (973) project, National Natural Science Foundation, 111 Project and Program for Changjiang Scholars and Innovative Research Team in University.

References

[1] V. Jong, R. Louw, Appl. Catal. A 271 (2004) 153.
[2] E.J. Shin, M.A. Keane, Appl. Catal. B 18 (1998) 241.
[3] M.A. Keane, G. Pina, G. Tavoularis, Appl. Catal. B 48 (2004) 275.
[4] N. Lingaiah, M.A. Uddin, A. Muto, T. Iwamoto, Y. Sakata, Y. Kusano, J. Mol. Catal. A 161 (2000) 157.
[5] M. Trillas, J. Peral, X. Domenech, J. Chem. Technol. Biotechnol. 67 (1996) 237.
[6] B.F. Hagh, D.T. Allen, in: H.M. Freeman (Ed.), Technomic, Lancaster, PA, 1990, p. 45.
[7] V.R.C. Komandur, V.R.R. Pendyala, V. Vishwanathan, Catal. Commun. 7 (2006) 974.
[8] D.G. Evans, R.C.T. Slade, Struct. Bond. 119 (2006) 1.
[9] D.Q. Li, Z.J. Tuo, D.G. Evans, X. Duan, J. Solid State Chem. 179 (2006) 3114.
[10] H.Y. Chen, F.Z. Zhang, S.S. Fu, X. Duan, Adv. Mater. 18 (2006) 3089.
[11] K.D. Vesely, A. Heights, R.S. Laurence, US Patent 3600129, 1971.
[12] Michalko, Edward, US Patent 3919117, 1976.
[13] N. Başar, L. Uzun, A. Güner, A. Denizli, Int. J. Biol. Macromol. 41 (2007) 234.
[14] Y. Zhao, F. Li, D.G. Evans, X. Duan, Chem. Mater. 14 (2002) 4286.
[15] V. Subramani, K.G. Santosh, Solid State Ionics 177 (2006) 803.
[16] E.J. Shin, A. Spiller, G. Tavoularis, M.A. Keane, Phys. Chem. Chem. Phys. 1 (1999) 3173.
[17] K.M. Parida, A.C. Pradhan, J. Das, N. Sahu, Mater. Chem. Phys. 113 (2009) 244.
[18] S.J. Gregg, K.S.W. Sing, Adsorption, Surface Area and Porosity, second ed., Academic Press, New York, 1982.
[19] J.T. Feng, Y.J. Lin, F. Li, D.G. Evans, D.Q. Li, Appl. Catal. A 329 (2007) 112.
[20] P.C. Bakala, E. Briot, Y. Millot, J.Y. Piquemal, J.M. Brégeault, J. Catal. 258 (2008) 61.
[21] F. Kovanda, T. Rojka, P. Bezdicka, K. Jiratovac, L. Obalova, K. Pacultova, Z. Bastl, T. Grygar, J. Solid State Chem. 182 (2009) 27.
[22] R. Molina, G. Poncelet, J. Phys. Chem. B 103 (1999) 11290.
[23] C.P. Li, A. Proctor, D.M. Hercules, Appl. Spectrosc. 38 (1984) 880.
[24] Z.F. Zhao, Z.J. Wu, L.X. Zhou, M.H. Zhang, W. Li, K.Y. Tao, Catal. Commun. 9 (2008) 2191.
[25] Z. Boukha, M. Kacimi, M.F.R. Pereira, J.L. Faria, J.L. Figueiredo, M. Ziyad, Appl. Catal. A 317 (2007) 299.
[26] E. Heracleous, A.F. Lee, K. Wilson, A.A. Lemonidou, J. Catal. 231 (2005) 59.
[27] V.R.C. Komandur, V.R.R. Pendyala, V.R. Vattikonda, Catal. Commun. 9 (2008) 886.
[28] A.G. Boudjahem, S. Monteverdi, M. Mercy, M.M. Bettahar, J. Catal. 221 (2004) 325.
[29] Y. Cesteros, P. Salagre, F. Medina, J.E. Sueiras, Appl. Catal. B 25 (2000) 213.
[30] R. Gopinath, N. Lingaiah, B. Sreedhar, I. Suryanarayana, P.S.S. Prasad, A. Obuchi, Appl. Catal. B 46 (2003) 587.
[31] R.A. Suzdorf, V.S. Morozov, N.N. Anshits, I.S. Tsiganova, G.A. Anshits, Catal. Lett. 29 (1994) 49.
[32] O. Orbay, S. Gao, B. Barbaris, E. Rupp, A.E. Saez, R.G. Arnold, E.A. Betterton, Appl. Catal. B 79 (2008) 43.